Journal of
Mateirals Chemistry A

Dynamic Article Links ►

This is the Pre-Published Version.

Cite this: DOI: 10.1039/c0xx00000x

ARTICLE TYPE

www.rsc.org/xxxxxx

A Rectification-Free Piezo-Supercapacitor with a Polyvinylidene Fluoride Separator and Functionalized Carbon Cloth Electrodes

Ruobing Song,[a] Huanyu Jin,[a] Xing Li,[a] Linfeng Fei,[a] Yuda Zhao,[a] Haitao Huang,[a] Helen Lai-Wa Chan,[a] Yu Wang*[a] and Yang Chai*[a]

Received (in XXX, XXX) Xth XXXXXXXXX 20XX, Accepted Xth XXXXXXXXX 20XX
DOI: 10.1039/b000000x

The integration of energy harvesting and energy storage device not only enables to convert ambient energy into electricity but also provides sustainable power source for various electronic devices and systems. It is highly desirable to improve the integration level and minimize unnecessary energy loss in the power-management circuits between energy harvesting and storage devices. In our work, we integrate a PVDF film into a supercapacitor as both the separator and the energy harvester. The double-sides of the polarized PVDF films are coated with H_2SO_4/poly(vinyl alcohol) (PVA) gel electrolyte. Functionalized carbon cloths are assembled with H_2SO_4/PVA electrolyte as both anode and cathode, forming a flexible all-solid-state supercapacitor. Externally mechanical impacts establish a piezoelectric potential across the PVDF films, and drive ions in the electrolyte to migrate towards the interface of the supercapacitor electrode, storing the electricity in the form of electrochemical energy. The asymmetric output characteristic of the piezoelectric PVDF film under mechanical impact results in the effective charging of the supercapacitor without any rectification device. The integrated piezo-supercapacitor shows the specific capacitance of 357.6 F/m^2, the power density of 49.67 mWh/m^2, and the energy density of 400 mW/m^2. Our hybridized energy harvesting and storage device can be further extended for providing sustainable power source of various types of sensors.

1. Introduction

Exploring renewable, sustainable, and green energy source is one of the most significative and challenging works to solve energy crises [1–4]. Energy harvesting and storage devices are becoming a key issue for the rapid developments of the energy system [5–11]. Energy harvesting device can convert the energy in other forms into the electricity but has limited energy storage. Usually, energy harvesting and storage devices are connected together by a power management circuit to enable sustainable power supply [12–21]. Piezoelectric materials can convert ubiquitously irregular and low-frequency mechanical vibration into electricity and have been extensively studied for the use of nanogenerator [22–30]. Owing to the excellent piezoelectricity and mechanical flexibility, poly-vinylidene fluoride (PVDF) film has been shown for the wearable and flexible energy generator[15–17,19,20,22,31–35].

For the integration of energy harvesting and storage devices, it is important to accumulate and store the harvested energy until a sufficient amount energy can be utilized for electronic devices and systems. In general, a full wave rectifier is used between the piezoelectric nanogenerator and the energy storage device, which decreases integration density and increases unnecessary energy loss. Recently, the self-charging power cell for one-step energy conversion and storage has been demonstrated with the integration of piezoelectric separator and Li-ion battery [36–38]. However, the Li-ion battery is usually limited by slow charging and poor cyclibility. Supercapacitor has gained immense attention as an effective energy storage device due to its higher charging rate, better cyclibility and higher power-density[18,39–44]. More recently, Ramadoss *et al.* have shown the integration of a pesuodo- supercapacitor and piezoelectric materials as a hybrid energy harvesting and storage device[26].

In this work, we demonstrate a hybrid piezo-supercapacitor involving the integration of both energy harvesting and storage. Our device consists of functionalized carbon cloth as the supercapacitor electrodes, PVDF film as the separator and energy harvester, and solid-state PVA as electrolyte. A polarized PVDF film is sandwiched between the symmetric carbon cloth electrodes and electrolyte. Externally mechanical impact establishes a piezoelectric potential across the PVDF film, which serves as a driving force for the migration of ions towards the interface of functionalized carbon cloth electrodes and stores the electricity in the form of electrochemical energy. We analyse the asymmetric output voltage of the piezoelectric PVDF. The amplitude difference during compress and relaxation enables the net charge of the supercapacitor

2. Experimental

2.1 Fabrication of the Poly vinyl alcohol (PVA)/H_2SO_4 electrolyte

PVA/H_2SO_4 electrolyte was prepared by mixing concentrated H_2SO_4, PVA powder and deionized water. A 3 g PVA powder (average molecular weight 130,000, Aldrich Chemistry) and 30 mL deionized water were mixed under 90 °C by constant stirring until a homogeneous solution was formed. After cooling down to room temperature, 3 g concentrated H_2SO_4 (97% Analytical grade) was added to the viscous solution.

2.2 Fabrication of the functionalized carbon cloth electrodes

Carbon cloth (1cm × 1cm × 0.025cm) was purchased from Fuel Cell Earth LLC as the supercapacitor electrode. The carbon cloth was cleaned and dried at room temperature in air. The detailed procedures of preparing the functionalized carbon cloth have been described elsewhere [39]. Briefly, it was functionalized by an anodic electrochemical method with a three-electrode cell system (a piece of carbon cloth with the area of 1.5 cm^2 as the working electrode, a graphite rod as the counter electrode and an Hg/Hg_2Cl_2 as the reference electrode). A voltage of 2.2 V was applied during the electrochemical process for 20 min in a 1M H_2SO_4 solution. The treated carbon cloth was subsequently cleaned by deionized water for several times and annealed in air at 200 °C for 3 hours.

2.3 Fabrication of the flexible piezo-supercapacitor

Polarized polyvinylidene fluoride (PVDF) films with a thickness of 100 μm were purchased from Jinzhou KeXin electronic materials Co. Ltd. A piece of PVDF film was cleaned with ethanol by ultrasonic cleaner and used as the separator of the supercapacitor. The PVDF film and two functionalized carbon clothes (FCC) were immersed in the PVA/H_2SO_4 electrolyte for 10 min and dried in air at room temperature. This coating process was repeated for 3 times. The PVDF film coated with PVA/H_2SO_4 was sandwiched between two FCC electrodes to form a symmetrical supercapacitor. The device was dried and solidified in air at room temperature over 8 hours. A supercapacitor without PVDF separator was also fabricated as a control sample.

2.4 Characterization

The morphologies of the materials were characterized using a scanning electron microscopy (SEM, JEOL JSM-633F). Raman spectroscopy (HORIBA HR800) with an excitation wavelength of 488 nm was used to measure the vibrational and rotational information about FCC and pure carbon cloth (PCC). The crystalline structures of the PVDF were investigated using an X-ray diffractometric (XRD, Rigaku Smartlab). The performance of the piezoelectric materials was measured by using an oscilloscope (Agilent Oscillator 3014a). Cyclic voltammetry and galvanostatic charge/discharge were carried out by using an electrochemical workstation (Shanghai Chenhua 660c). The charging/discharging properties of the piezo-supercapacitor were characterized by a Keithely 2410 source meter.

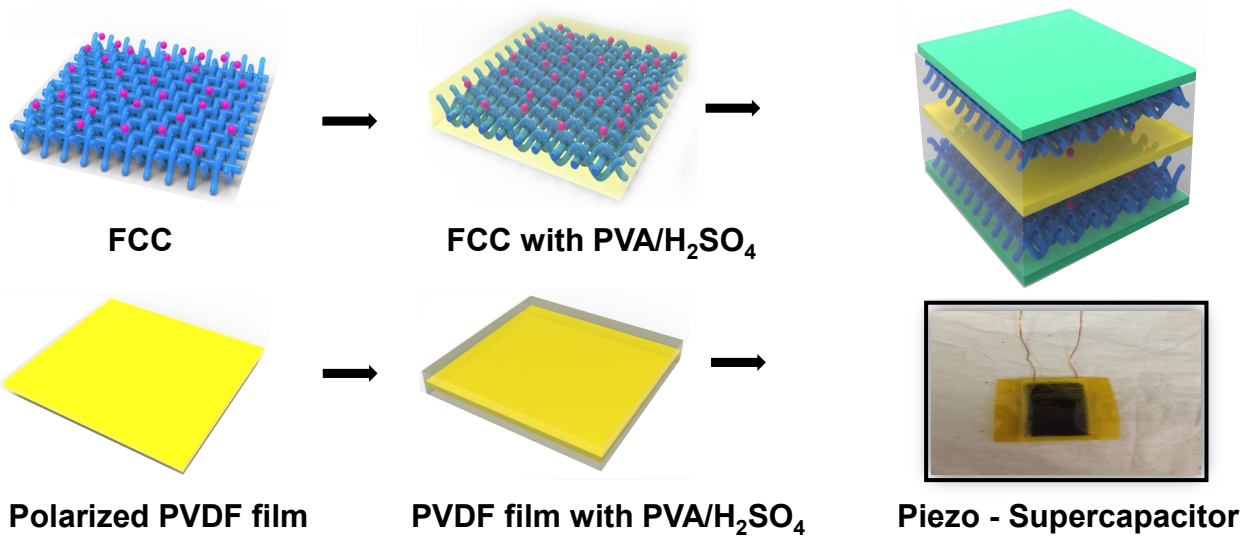

Fig. 1 Schematic illustration of the process flow of the hybrid piezo-supercapacitor. PVDF separator and functionalized carbon cloth electrodes are coated with PVA/H_2SO_4 electrolyte, and assembled together.

3. Results and Discussions

Figure 1 shows the schematic process flow of fabricating the flexible piezo-supercapacitor. We used FCC as the supercapacitor electrode because its excellent mechanical stability and intrinsic flexibility allow it to withstand intensely mechanical vibration. The macroscopic porous structure of the carbon cloth also enhances the intimate contact between the electrodes and electrolytes, which favors the diffusion of ions and the transportation of electrons in the bulk electrode. A simple oxidation and annealing method has been demonstrated as an effective way to introduce various functional groups on the carbon cloth and increase the capacitance by the redox reactions

of these functional groups [39]. The PVDF film sandwiched between the two FCC electrodes serves as not only the separator of the supercapacitor but also the piezoelectric energy harvester, which can convert mechanical vibration into electricity. A voltage potential can be generated across the piezoelectric PVDF under externally mechanical vibration. The built-in electric-field across the PVDF film can drive the ions in the electrolyte to migrate towards the interface of the symmetric FCC electrodes, establishing an electronic double layer or pseudo-capacitance at the interface and storing the electricity in the form of electrochemical energy [39].

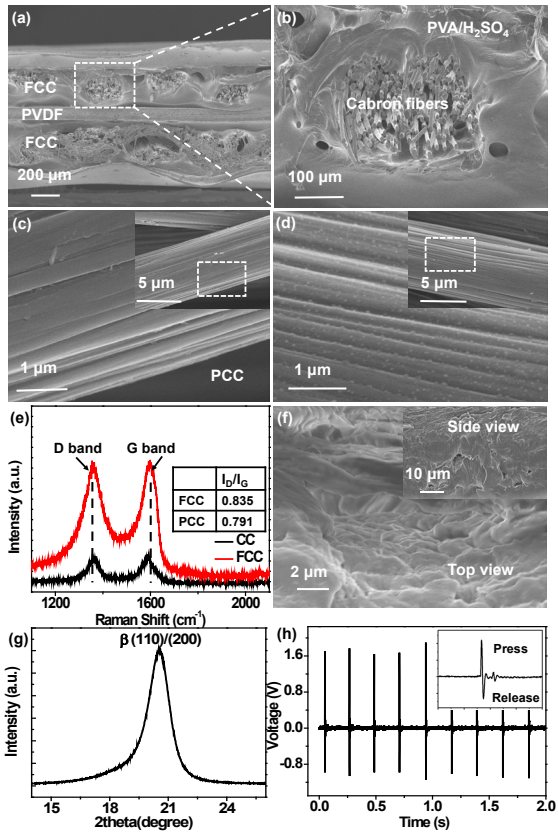

Fig. 2 SEM images of (a) the cross section of the piezo-supercapacitor, which consists of symmetric FCC electrodes and piezoelectric PVDF film as a separator and energy harvester. (b) Enlarged view of the functional carbon fibers surrounded by the PVA/H_2SO_4 electrolyte. Enlarged SEM images of (c) the PCC and (d) the FCC. Inset: high-magnification SEM image, which can be seen that the functional groups are attached on the surface of carbon cloth. (e) Raman spectra of FCC and PCC. (f) Top view SEM image of the PVDF film. The inset shows the cross-sectional SEM image. (g) The XRD pattern of the PVDF with β-phase (110/200), indicating that the PVDF is fully polarized. (h) The voltage output profiles of PVDF separator with opposite polarization under a periodic mechanical compressive straining. Enlarged image of (h) shows the opposite output during once stress applied, which is due to the difference in strain rate of the PVDF film when be compressed and released.

Figure 2(a) shows a cross-sectional scanning electron microscopy (SEM) image of the sandwiched structure. The enlarged view in **Figure 2(b)** shows that the carbon fibers in the electrode are fully surrounded with PVA/H_2SO_4 electrolyte. **Figure 2(c)** and **2(d)** are the SEM images of the carbon cloth before and after the functionalization, respectively. After the oxidation and annealing processes, a lot of particle-like dots uniformly distributed on the surface of FCC fibers, which were not observed in pure carbon cloth (PCC). We suppose that these are possibly resulted from the carbonyl, hydroxyl, and carboxylic functional groups. In order to further investigate the structure changes in functionalized carbon cloth, we characterized the samples using Raman spectroscopy, as shown in **Figure 2 (e)**. The two strong peaks at 1350 cm^{-1} and 1580 cm^{-1} are corresponding to the D band and G band of carbon, respectively. The D band is often referred to the disorder or defect in the carbon, and the G band usually is related to sp^2 carbon-carbon bonding. The table in the inset of **Figure 2 (e)** shows the intensity ratio of D band to G band. The I_D/I_G of the FCC is higher than that of the PCC, indicating that more structural defects are generated in the functionalization process. **Figure 2(f)** and the insert figures are typical top-view and cross-sectional SEM image of the PVDF film, showing the porous structure. **Figure 2(g)** shows the X-ray diffraction (XRD) pattern of the PVDF film. The peak of (1 1 0 / 2 0 0) indicates that the PVDF film is fully polarized β ferroelectric phase. To investigate the piezoelectric performance of the PVDF films, we coated both sides of the polarized PVDF films with an Au layer and measured the output voltage and current. **Figure 2(h)** is the output voltage profiles of the PVDF film under a periodic compressive force with average frequency of 4.5 Hz. According to the results, the compressive force produces an output voltage with two opposite polarity peaks. The positive peak corresponds to the stage under compressive forces, while the negative peak represents for the stage of natural relaxation process. The different duration of the two stages gives rise to the asymmetric characteristics of the amplitude in the two peaks, which enables to charge the supercapacitor without a rectification unit. According to the piezoelectricity theory, the generated current of the piezoelectric material under external vibration is proportional to the applied strain rate, as shown in equation (1)[33]:

$$\frac{dQ}{dt} = d_{33} EA \frac{d\epsilon}{dt} \quad (1)$$

where Q is the generated charge of piezoelectric generator, t is time duration, d_{33} is the piezoelectric constant, E is the Young's modulus, A is the cross-sectional area, and ε is the applied strain. The strain rate during the relaxation process is relative lower than that during the compressive process by external impact. The generated electric-field in the relaxation process has opposite direction and smaller amplitude compared with the compressive process. Therefore, the charging process is dominated by the compressive process by the mechanical impact. **Figure S1** shows the output voltage profile of the PVDF film with the opposite polarization. In addition, the magnitude of the piezoelectric potential is linearly proportional to the magnitude of applied force [36–38]. The intensely mechanical impact will results in strong built-in electric-field.

Figure 3(a) shows the cyclic voltammetry (CV) curves of the symmetric supercapacitors with FCC electrodes and PCC electrodes with the sweep rate of 100 mV/s. The CV curve of the supercapacitor with the PCC electrodes shows almost negligible capacitance. The CV curve of the supercapacitor with the FCC electrodes shows rectangular shape within the operation voltage range of 0-1 V, suggesting that the FCC electrode exhibits

significant improvement of the capacity. After the functionalization, the areal capacitance of the carbon cloth electrode is increased by 214 times. These results demonstrate that the anodic electrochemical oxidation process is an effective and simple method to increase the capacitance by orders of magnitude of carbon-based electrodes. This outstanding performance of the FCC electrode is mainly ascribed to the

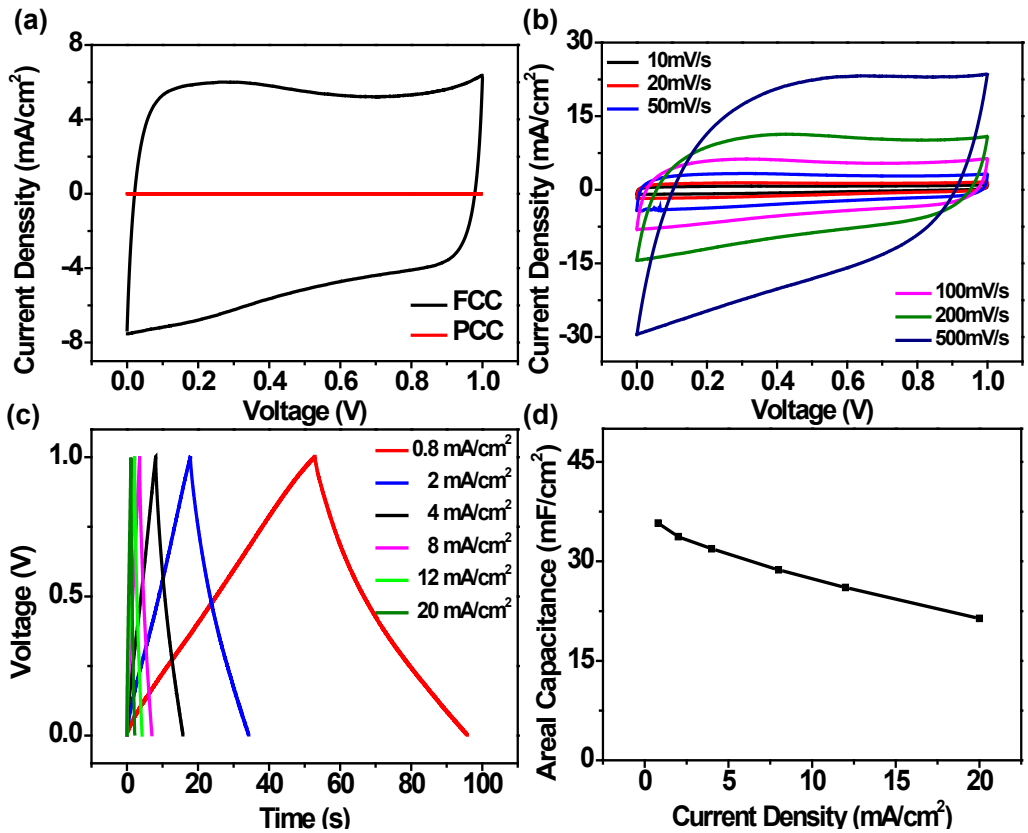

Fig. 3 Electrochemical characterization of the supercapacitors. (a) Cyclic voltammograms curves measured at a scan rate of 100 mV/s for the supercapacitor with symmetric PCC and FCC electrodes. (b) CV curves of the FCC supercapacitor with the PVDF separator measured at scan rates of 10, 20, 50, 100, 200, and 500 mV/s. (c) Galvanostatic charging and discharging curves of the piezo-supercapacitor measured at different current densities from 8 to 200 A/m^2. (d) Calculated areal capacitance of the supercapacitor with and without PVDF separator based on galvanostatic charging-discharging current density.

Faradaic reaction of these $>C=O$, $>COH$ and $-COOH$ functional group[39]:

$$>COH \Leftrightarrow >C=O + H^+ + e^- \quad (2)$$

$$-COOH \Leftrightarrow -COO + H^+ + e^- \quad (3)$$

$$>C=O + e^- \Leftrightarrow >C-O^- \quad (4)$$

In addition, the electrochemical performance of the FCC electrodes is also affected by the annealing temperature. With the annealing temperature increased from room temperature to 100 ℃, 200 ℃, and 300 ℃, the amount of the functional groups decreased and the conductivity of FCC was increased. Good electrical conductivity is helpful to achieve high charging/discharging rate. But the decrease of functional groups also reduces the capacity. Thus, the annealing temperature plays an important role to balance the conductivity and the capacity of the supercapacitor electrode. In this work, we used the FCC electrodes annealed at 200 ℃ as the supercapacitor electrode.

Figure 3(b) shows the CV curves of the piezo-supercapacitor with the PVDF separator. The shape of the CV curves is quasi-rectangular at different scan rates, ranging between 10 and 500 mV/s, indicating good electrochemical properties of the supercapacitor. **Figure S2(a)** shows the CV curves of the supercapacitor without the PVDF separator and exhibits similar behavior with that of the piezo-supercapacitor. **Figure 3(c)** shows the galvanostatic charge–discharge (GCD) curves of the piezo-supercapacitor, which was conducted between 0 and 1V at different charge/discharge current densities. The device shows a stable isosceles triangle shape even at high current density, which confirming again an excellent capacitive behavior. The GCD curves of supercapacitor without PVDF separator are shown in **Figure S2(b).** The areal capacitance (C_m) of piezo-supercapacitor was calculated according to the equation (5):

$$Cm = \frac{I \times \Delta t}{S \times \Delta V} \quad (5)$$

where C_m is the areal capacitance, I is the discharge current, Δt is the discharge time, S is the effective area of the FCC electrodes (~ 1 cm^2), ΔV is the potential range during the discharge process. According to **Figure 3(d)**, the extracted areal capacitances of supercapacitor with PVDF separator are 357.6, 337.2, 318.8, 287.2, 260.4, 214 F/m^2 at the current densities of 8, 20, 40, 80, 100, 120, 200 A/m^2, respectively. The maximum specific capacitance of 357.6 F/m^2 is obtained at the current density of 8 A/m^2. More importantly, it exhibits a relatively good charge/discharge rate capability, retaining 59.84% of the capacitance when the current density increased from 8 to 200 A/m^2. **Figure S2(c)** shows the calculated areal capacitance of the supercapacitor with and without the PVDF film. These results suggest that the electrochemical properties of the supercapacitor with the PVDF separator are comparable to those without it. The highest areal energy density E of the device calculated based on GCD curve is 49.67 mWh/m^2, and the power density of the device is 400 mW/m^2, indicating comparatively good power output ability. **Figure S2(d)** shows the CV curves of the piezo-supercapacitor under different mechanical deformation states (flat, bent and twisted), exhibiting negligible difference and indicating excellent mechanical flexibility

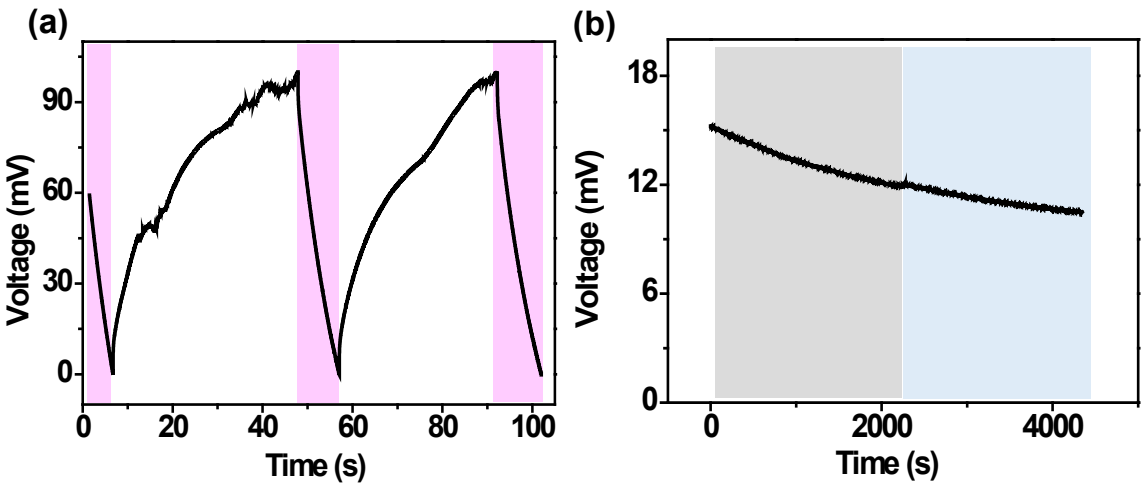

Fig. 4 Self-charging performance of the supercapacitors. (a) Typical self-charging process performance of a piezo-supercapacitor. (b) The PVDF separator was replaced with commonly used NKK. No self-charging effect was observed.

Figure 4(a) shows a typical charging process of the piezo-supercapacitor. At first, the initial voltage of the device was discharged to zero under a constant current of 100 μA. After that, the charging process was under a continuous compressive force with the average frequency of 4.5 Hz. Then, the device was discharged at a constant current of 100 μA again. According to these results, the voltage of the supercapacitor was increased to 100 mV within 40 s. Based on the calculation of the discharging curve, the stored electric capacity was about 0.25 μAh. The piezo-supercapacitor showed an areal capacitance of 100 F/m^2, almost 30% of the areal capacitance of supercapacitor which is charged by external power source. The energy density and power density of the piezo-supercapacitor charged by mechanical force are 0.278 mWh/m^2 and 0.028 mW/m^2.

To confirm that the increased voltage of the supercapacitor is resulted from the piezoelectric separator, we replaced the PVDF film with a commonly used separator without piezoelectric properties (NKK TF40, 40 μm thickness) and measured the voltage response under the same periodic force condition. **Figure 4(b)** shows the corresponding result. During the stage of the initial 2000 s without any external forces, the device shows the leakage characteristics. In the following 2000 s with a repeated compressive force, the device still keeps the linearly decrease rate and cannot be charged up at all. Therefore, the supercapacitor without piezoelectric separator cannot be charged by applying a repeatable mechanical deformation. This indicates that the charging of the supercapacitor is truly resulted from the piezoelectric PVDF separator.

PVDF is widely investigated due to its excellent mechanical flexibility and high piezoelectric constant. The β phase PVDF exhibits remarkably piezoelectric properties [45]. The working mechanism of the piezo-supercapacitor is shown in **Figure 5**. At the beginning, the piezoelectric PVDF film is sandwiched between symmetric FCC electrodes, and surrounded with PVA/H_2SO_4 electrolyte, as shown in **Figure 5(a).** It is noteworthy that the free-standing supercapacitor piezoelectric PVDF has an initial voltage of 60 ~ 90 mV instead of zero potential. This initial voltage is possibly caused by the remnant polarization of the PVDF film, which can be induced by the polling process or further increased by compressive stress during the fabrication process. When the electrolyte is intimately contacted with the PVDF film, the charge will be electrostatically induced by the remnant polarization at the interface between the electrolyte and the PVDF. When the piezo-supercapacitor is subjected to a periodic compressive stress, the remnant polarization of the PVDF film is changed, as shown in **Figure 5(b)**. To balance the changed remnant polarization, charge carriers will be drifted towards the electrode of the supercapacitor. Two factors affect the charging process. First, the increased bonded charge density of the PVDF surface influences the distribution of the positive ions and negative ions in electrolyte. The piezo-potential gives rise to the redistribution of the ions and accumulates the charges on the surface of supercapacitor electrode. Second, the piezo-potential will drive the migration hydrogen ion (H^+) and SO_4^{2-} along the direction of the potential across the porous PVDF film [26,38]. With the increase

of the potential between the positive and negative electrodes, more electricity is stored on the electrodes in the form of electrochemical energy. After the H^+ ions and SO_4^{2-} ions redistribute in the electrolyte and balance the piezoelectric field in the PVDF film, the non-faradic and faradic force of the two electrodes reach a new equilibrium, as schematically shown in **Figure 5(c)**. When the applied compressive stress is released, one self-charging cycle is completed. **Figure 5(d)** shows the schematic of the piezo-supercapacitor is under the relaxation stage. A reversed piezoelectric filed was created when the compressive force removed, but the value of the magnitude of created during compressive process, because the stain rate in the relaxation process is smaller than that in compressive process. Therefore, the reversed piezoelectric field cannot counteract the overall charging process. Thus, the hybrid piezo-supercapacitor can be successfully charged as long as the frequency of the mechanical vibration is larger than a critical value. It is true that the reversed electric-field degrades the energy conversion efficiency of the integrated device. But the elimination of the use of rectification part greatly enhances the integration level of the energy harvesting/storage system. When the device is mechanically deformed again, the process presented above is

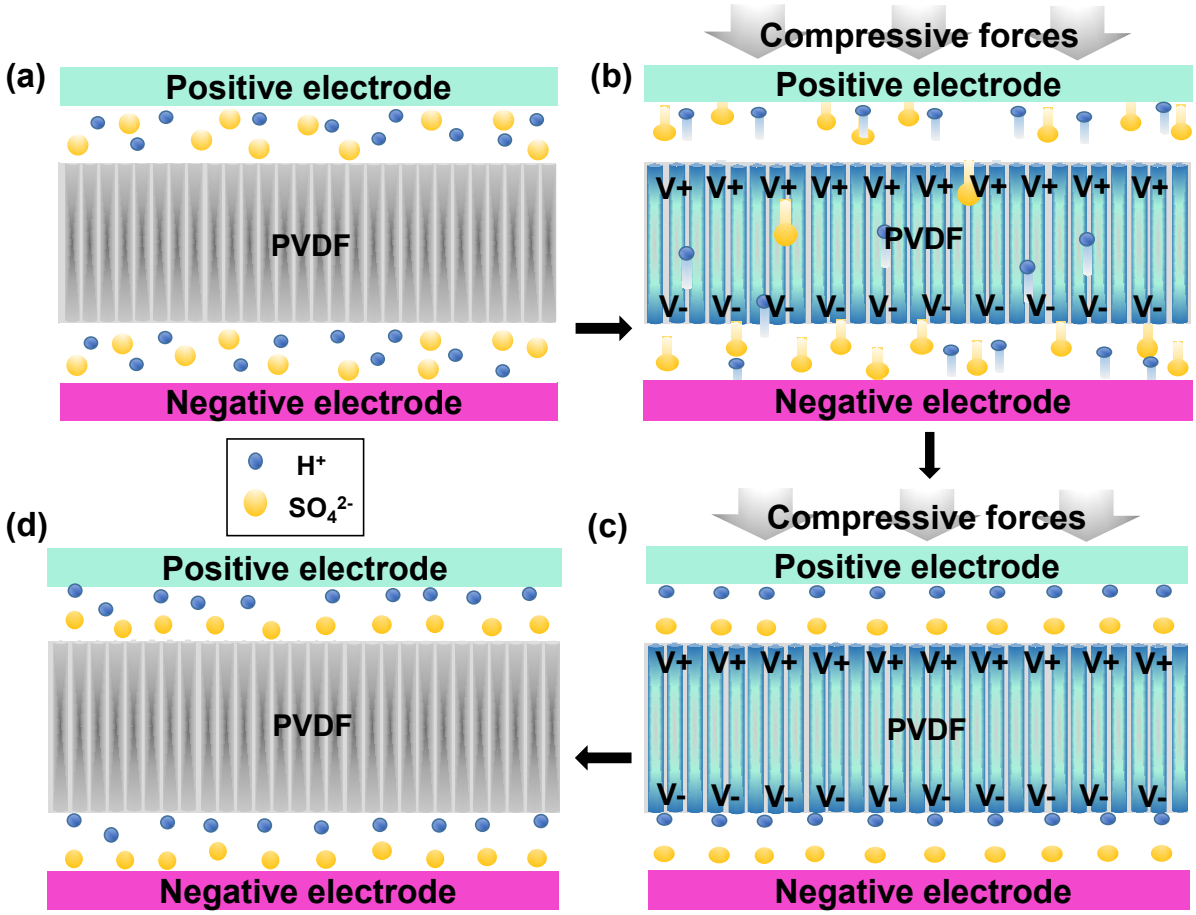

this reversed electric-field is around 2 times smaller than that repeated.

Fig. 5 Proposed working mechanism of the hybrid piezo-supercapacitor. (a) Original condition after the fabrication process. (b) The device is under compressive stress. PVDF film creates a piezoelectric field drive the migration of ions. (c) A new equilibrium state is reached between electrochemical and piezoelectric potential. (d) Completed one self-charging cycle.

Conclusions

In summary, we successfully fabricated a rectification-free piezo-supercapacitor, which integrates both supercapacitor and piezoelectric energy harvesting film. The flexible piezoelectric PVDF film can convert mechanical vibration into a built-in electric-field, which serves as the driving force for the migration of ions towards the interface of the FCC electrodes. The asymmetric characteristics of the PVDF film during compress and relaxation stages results in the effective charging without any rectification device. The flexible piezo-supercapacitor exhibits that it can maintain high mechanical strength and high capacitance simultaneously under the bending and stretching test, and shows stable electrochemical performance with energy density 49.67 mWh/m^2 and power density 400 mW/m^2. Our device can be further extended for providing sustainable power source of various types of sensors.

Acknowledgement

We acknowledge financial support from the Research Grant Council of Hong Kong (grant number: PolyU 252001/14E), the Hong Kong Polytechnic University (grant numbers: G-UA51, 1-

ZVCG, G-UC71), and the High-tech Program ("863") of China-2013AA031903.

Notes and references

[a] *Department of Applied Physics, The Hong Kong Polytechnic University, Hung Hom, Kowloon, Hong Kong, People's Republic of China. E-mail: ychai@polyu.edu.hk, yuwang@polyu.edu.hk*

† Electronic Supplementary Information (ESI) available: the output voltage profile of the PVDF film with the opposite polarization; CV curves and GCD curves of the supercapacitor without the PVDF separator; the calculated areal capacitance of the supercapacitor with and without the PVDF film; CV curves of the piezo-supercapacitor under different mechanical deformation states (flat, bent and twisted); Piezo-supercapacitor charging base on initial voltage are included.. See DOI: 10.1039/b000000x/

1 B. Huskinson, M. P. Marshak, C. Suh, S. Er, M. R. Gerhardt, C. J. Galvin, X. Chen, A. Aspuru-Guzik, R. G. Gordon and M. J. Aziz, *Nature*, 2014, **505**, 195–198.
2 Z. Zou, J. Ye, K. Sayama and H. Arakawa, *Nature*, 2001, **414**, 625–627.
3 O. Gutfleisch, M. A. Willard, E. Brück, C. H. Chen, S. G. Sankar and J. P. Liu, *Adv. Mater.*, 2011, **23**, 821–842.
4 W. Tu, Y. Zhou and Z. Zou, *Adv. Mater.*, 2014, **26**, 4607–4626.
5 J. Cabana, L. Monconduit, D. Larcher and M. R. Palacín, *Adv. Mater.*, 2010, **22**, E170–E192.
6 X. Cai, M. Peng, X. Yu, Y. Fu and D. Zou, *J. Mater. Chem. C*, 2014, **2**, 1184–1200.
7 L. Dai, *Acc. Chem. Res.*, 2013, **46**, 31–42.
8 M. F. El-Kady and R. B. Kaner, *Nat. Commun.*, 2013, **4**, 1475–1484.
9 Y. G. Guo, J. S. Hu and L. J. Wan, *Adv. Mater.*, 2008, **20**, 2878–2887.
10 N. G. Sahoo, Y. Pan, L. Li and S. H. Chan, *Adv. Mater.*, 2012, **24**, 4203–4210.
11 Y. Wang, T. Wang, P. Da, M. Xu, H. Wu and G. Zheng, *Adv. Mater.*, 2013, **25**, 5177–5195.
12 D. Karabelli, J. C. Leprêtre, F. Alloin and J. Y. Sanchez, *Electrochim. Acta*, 2011, **57**, 98–103.
13 K. Hwang, B. Kwon and H. Byun, *J. Memb. Sci.*, 2011, **378**, 111–116.
14 H. a. Sodano, *J. Intell. Mater. Syst. Struct.*, 2005, **16**, 799–807.
15 A. Gheibi, M. Latifi, A. A. Merati and R. Bagherzadeh, *J. Polym. Res.*, 2014, **21**, 1–7.
16 T. Park, B. Kim, Y. Kim and E. Kim, *J. Mater. Chem. A*, 2014, **2**, 5462–5469.
17 S. Bae, O. Kahya, B. K. Sharma, J. Kwon and H. J. Cho, *ACS Nano*, 2013, **4**, 3130–3138.
18 Y. Xie, Y. Liu, Y. Zhao, Y. H. Tsang, S. P. Lau, H. Huang and Y. Chai, *J. Mater. Chem. A*, 2014, **2**, 9142–9149.
19 X. Wen, W. Yang, Q. Jing and Z. L. Wang, *ACS Nano*, 2014, **8**, 7405–7412.
20 J.-H. Lee, K. Y. Lee, B. Kumar, N. T. Tien, N. Lee and S.-W. Kim, *Energy Environ. Sci.*, 2013, **6**, 169–175.
21 Z. Li, X. Zhang and G. Li, *Phys. Chem. Chem. Phys.*, 2014, **16**, 5475–5479.
22 R. Hinchet, S. Lee, G. Ardila, L. Montès, M. Mouis and Z. L. Wang, *Adv. Funct. Mater.*, 2014, **24**, 971–977.
23 Y. Hu and Z. L. Wang, *Nano Energy*, 2015.
24 K. Il Park, J. H. Son, G. T. Hwang, C. K. Jeong, J. Ryu, M. Koo, I. Choi, S. H. Lee, M. Byun, Z. L. Wang and K. J. Lee, *Adv. Mater.*, 2014, **26**, 2514–2520.
25 K. C. Pradel, W. Wu, Y. Ding and Z. L. Wang, *Nano Lett.*, 2014, **14**, 6897–6905.
26 A. Ramadoss, B. Saravanakumar, S. W. Lee, Y.-S. Kim, S. J. Kim and Z. L. Wang, *ACS Nano*, 2015, **9**, 4337–4345.
27 C. H. Wang, W. S. Liao, Z. H. Lin, N. J. Ku, Y. C. Li, Y. C. Chen, Z. L. Wang and C. P. Liu, *Adv. Energy Mater.*, 2014, **4**, 1400392–1400399.
28 X. Xue, Y. Nie, B. He, L. Xing, Y. Zhang and Z. L. Wang, *Nanotechnology*, 2013, **24**, 225501–225507.
29 R. Yu, C. Pan, J. Chen, G. Zhu and Z. L. Wang, *Adv. Funct. Mater.*, 2013, **23**, 5868–5874.
30 J. Zhong, Y. Zhang, Q. Zhong, Q. Hu, B. Hu, Z. L. Wang and J. Zhou, *ACS Nano*, 2014, **8**, 6273–6280.
31 S. R. Anton and H. A. Sodano, *Smart Mater. Struct.*, 2007, **16**, R1–R21.
32 C. R. Bowen, H. a. Kim, P. M. Weaver and S. Dunn, *Energy Environ. Sci.*, 2014, **7**, 25–44.
33 C. Chang, V. H. Tran, J. Wang, Y. K. Fuh and L. Lin, *Nano Lett.*, 2010, **10**, 726–731.
34 G. K. Ottman, H. F. Hofmann, A. C. Bhatt and G. A. Lesieutre, *IEEE Trans. Power Electron.*, 2002, **17**, 669–676.
35 Y. Qin, X. Wang and Z. L. Wang, *Nature*, 2008, **451**, 809–813.
36 L. Xing, Y. Nie, X. Xue and Y. Zhang, *Nano Energy*, 2014, **10**, 44–52.
37 X. Xue, P. Deng, B. He, Y. Nie, L. Xing, Y. Zhang and Z. L. Wang, *Adv. Energy Mater.*, 2014, **4**, 1301329–1301334.
38 X. Xue, S. Wang, W. Guo, Y. Zhang and Z. L. Wang, *Nano Lett.*, 2012, **12**, 5048–5054.
39 L. Hu, M. Pasta, F. La Mantia, L. Cui, S. Jeong, H. D. Deshazer, J. W. Choi, S. M. Han and Y. Cui, *Nano Lett.*, 2010, **10**, 708–714.
40 W. M. Tang, H. Y. Jin, Z. H. Peng and H. Chan, *RSC Adv.*, 2014, **4**, 33022–33028.
41 L. L. Zhang and X. S. Zhao, *Chem. Soc. Rev.*, 2009, **38**, 2520–2531.
42 Y. Zhu, S. Murali, M. D. Stoller, K. J. Ganesh, W. Cai, P. J. Ferreira, A. Pirkle, R. M. Wallace, K. A. Cychosz, M. Thommes, D. Su, E. A. Stach and R. S. Ruoff, *Science*, 2011, **332**, 1537–1541.
43 S. Wang, R. Dryfe, *J. Mater. Chem. A, 2013,**1**, 5279-5283.*
44 S. Wang, B. Pei, X. S. Zhao, R. Dryfe, *Nano Energy,* 2013, **2**, 530
45 *L. Li, M. Zhang, M. Rong and W. Ruan, RSC Adv., 2014, **4**, 3938–3943.*